
AFRL-RX-WP-TP-2010-4060

# ON THE NUCLEATION AND GROWTH OF α-Ti OFF OF TiB PRECIPITATES (PREPRINT)

**T.T. Sasaki, B. Fu, K. Torres, and G.B. Thompson**

**The University of Alabama**

**R. Srinivasan**

**Wright State University**

**J.S.Tiley**

**Metals Branch**
**Metals, Ceramics & NDE Division**

**JANUARY 2010**

**Approved for public release; distribution unlimited.**

***See additional restrictions described on inside pages***

**STINFO COPY**

**AIR FORCE RESEARCH LABORATORY**
**MATERIALS AND MANUFACTURING DIRECTORATE**
**WRIGHT-PATTERSON AIR FORCE BASE, OH 45433-7750**
**AIR FORCE MATERIEL COMMAND**
**UNITED STATES AIR FORCE**

# REPORT DOCUMENTATION PAGE

*Form Approved*
*OMB No. 0704-0188*

The public reporting burden for this collection of information is estimated to average 1 hour per response, including the time for reviewing instructions, searching existing data sources, gathering and maintaining the data needed, and completing and reviewing the collection of information. Send comments regarding this burden estimate or any other aspect of this collection of information, including suggestions for reducing this burden, to Department of Defense, Washington Headquarters Services, Directorate for Information Operations and Reports (0704-0188), 1215 Jefferson Davis Highway, Suite 1204, Arlington, VA 22202-4302. Respondents should be aware that notwithstanding any other provision of law, no person shall be subject to any penalty for failing to comply with a collection of information if it does not display a currently valid OMB control number. **PLEASE DO NOT RETURN YOUR FORM TO THE ABOVE ADDRESS**.

| 1. REPORT DATE *(DD-MM-YY)* | 2. REPORT TYPE | 3. DATES COVERED *(From - To)* |
|---|---|---|
| January 2010 | Journal Article Preprint | 01 January 2010 – 31 January 2010 |

**4. TITLE AND SUBTITLE**
ON THE NUCLEATION AND GROWTH OF α-Ti OFF OF TiB PRECIPITATES (PREPRINT)

**5a. CONTRACT NUMBER**
In-house

**5b. GRANT NUMBER**

**5c. PROGRAM ELEMENT NUMBER**
62102F

**6. AUTHOR(S)**
T.T. Sasaki, B. Fu, K. Torres, and G.B. Thompson (The University of Alabama)
R. Srinivasan (Wright State University)
J.S.Tiley (AFRL/RXLM)

**5d. PROJECT NUMBER**
4347

**5e. TASK NUMBER**
RG

**5f. WORK UNIT NUMBER**
M02R1000

**7. PERFORMING ORGANIZATION NAME(S) AND ADDRESS(ES)**
The University of Alabama
Department of Metallurgical & Materials Engineering
Box 870202
Tuscaloosa, AL 35487-0202
---
Wright State University
Mechanical & Materials Engineering Department
3640 Colonel Glenn Highway
Dayton, OH 45435

Metals Branch (AFRL/RXLM)
Metals, Ceramics & NDE Division
Materials and Manufacturing Directorate
WPAFB, OH 45433-7750
Air Force Materiel Command
United States Air Force

**8. PERFORMING ORGANIZATION REPORT NUMBER**
AFRL-RX-WP-TP-2010-4060

**9. SPONSORING/MONITORING AGENCY NAME(S) AND ADDRESS(ES)**
Air Force Research Laboratory
Materials and Manufacturing Directorate
Wright-Patterson Air Force Base, OH 45433-7750
Air Force Materiel Command
United States Air Force

**10. SPONSORING/MONITORING AGENCY ACRONYM(S)**
AFRL/RXLMD

**11. SPONSORING/MONITORING AGENCY REPORT NUMBER(S)**
AFRL-RX-WP-TP-2010-4060

**12. DISTRIBUTION/AVAILABILITY STATEMENT**
Approved for public release; distribution unlimited.

**13. SUPPLEMENTARY NOTES**
Journal article submitted to Materials Science and Engineering. PAO Case Number: 88ABW-2010-0179; Clearance Date: 15 Jan 2010. Paper contains color.

**14. ABSTRACT**
We have investigated the microstructure of the β-stabilized Ti-15Mo-2.6Nb-3Al-0.2Si-0.12B alloy at two different aging temperatures, 540 ◦C/8 hr and 660 ◦C/8 hr. At the lower aging temperature, α-Ti precipitated as needle-like shapes off of the TiB phase. In contrast, the higher aged sample exhibited globular α-Ti morphology around the TiB phase. This difference has been rationalized by the coarsening behavior of α-Ti around the TiB phase. Various orientation relationships were observed between these two samples. This difference is because the precipitation of α-Ti off of two different TiB planes. In addition, atom probe analysis confirmed the segregation of alpha and beta stabilizing elements to the respective phases. It was noted that silicon enriched the α-Ti/β-Ti interface at the lower aged temperature where as this enrichment was observed at the α-Ti/TiB interface at the higher aged temperature.

**15. SUBJECT TERMS**
Ti-15Mo-2.6Nb-3Al-0.2Si alloy, α-Ti, TiB, TEM and 3D atom probe

| 16. SECURITY CLASSIFICATION OF: | | | 17. LIMITATION OF ABSTRACT: | 18. NUMBER OF PAGES | 19a. NAME OF RESPONSIBLE PERSON (Monitor) |
|---|---|---|---|---|---|
| a. REPORT | b. ABSTRACT | c. THIS PAGE | | | Christopher F. Woodward |
| Unclassified | Unclassified | Unclassified | SAR | 32 | 19b. TELEPHONE NUMBER *(Include Area Code)* N/A |

**Standard Form 298 (Rev. 8-98)**
Prescribed by ANSI Std. Z39-18

# On the Nucleation and Growth of α-Ti off of TiB Precipitates

T. T. Sasaki[1)], B. Fu[1)], K. Torres[1)] G.B. Thompson[1,#)], R. Srinivasan[2)] and J. Tiley[3)]

[1)] The University of Alabama, Department of Metallurgical & Materials Engineering, Box 870202, Tuscaloosa, AL 35487-0202

[2)] Wright State University, Mechanical & Materials Engineering Department, 3640 Colonel Glenn Highway, Dayton, OH 45435

[3)] Air Force Research Laboratory, Wright-Patterson Air Force Base, Dayton, OH 45431

# contact author: gthompson@eng.ua.edu

**Abstract**

We have investigated the microstructure of the β-stabilized Ti-15Mo-2.6Nb-3Al-0.2Si-0.12B alloy at two different aging temperatures, 540 $^{o}$C/8 hr and 660 $^{o}$C/8 hr. At the lower aging temperature, α-Ti precipitated as needle-like shapes off of the TiB phase. In contrast, the higher aged sample exhibited globular α-Ti morphology around the TiB phase. This difference has been rationalized by the coarsening behavior of α-Ti around the TiB phase. Various orientation relationships were observed between these two samples. This difference is because the precipitation of α-Ti off of two different TiB planes. In addition, atom probe analysis confirmed the segregation of alpha and beta stabilizing elements to the respective phases. It was noted that silicon enriched the α-Ti/β-Ti interface at the lower aged temperature where as this enrichment was observed at the α-Ti/TiB interface at the higher aged temperature.

Keywords: Ti-15Mo-2.6Nb-3Al-0.2Si alloy, α-Ti, TiB, TEM and 3D atom probe

## 1. Introduction

The low density coupled with mechanical strength of titanium alloys have made them candidate materials for aerospace and automotive applications. In particular, metastable β-Ti alloys provide superior mechanical properties with good machinability as compared to other titanium alloys. The heat treatable Ti-15Mo-2.6Nb-3Al-0.2Si (wt.%) alloy (β-21S) is a low cost β-Ti alloy which offers high specific strength over a wide range of temperatures **[1-3]**. This is because of the dispersion of lath-like hexagonal close packed (hcp) α-Ti precipitates dispersed within the body centered cubic (bcc) β-Ti matrix.

In order to disperse the α-Ti precipitates during the aging, solution heat treatments above the β-transus temperature (~ 800 ºC) need to be performed prior to the aging treatment in order to dissolve the α-Ti phase into the β-Ti matrix **[4]**. However, at such high temperature heat treatments, a degradation of the mechanical properties can occur because of significant grain growth. Cherukuri *et al*. **[5]** recently reported that a dispersion of thermally stable titanium-boride particles, formed by trace boron additions, was effective in restricting the grain growth during the high temperature heat treatment of the Ti-15Mo-2.6Nb-3Al-0.2Si (wt.%) alloy. Similar effects have been noted in other Ti-based alloys that were reinforced by the TiB phase **[6-13]**. The boride particles act as the pinning sites for the grain boundaries. In the TiB reinforced Ti-6Al-4V alloy, these titanium-boride particles provide additional nucleation sites for the α-Ti precipitates in addition to the α-Ti precipitates that form along the grain boundaries into the Widmanstätten microstructure **[14]**. In the Ti-6Al-4V alloy reinforced by TiB particles, the α-Ti precipitates that nucleated at the TiB particles have an equi-axed shape, and the morphology is different from those present along the β-Ti grain boundaries. This TiB/α-Ti orientation relationship in Ti-6Al-4V has been reported to be

$(001)_{TiB}$ //$(0001)_{\alpha-Ti}$ , $[010]_{TiB}$ //$[11\bar{2}0]_{\alpha-Ti}$ **[14, 15]**. To date, there has been little to no work reporting the orientation relationship or micro-segregation that occurs during α-Ti precipitation on TiB in the Ti-15Mo-2.6Nb-3Al-0.2Si alloy. An understanding of the potential microstructural evolution differences between these two systems will provide insights necessary for optimizing the ductility of these alloys. In this work, we have investigated the α-Ti phase nucleating at TiB precipitates via scanning electron microscopy (SEM), transmission electron microscopy (TEM) and 3D atom probe (3DAP).

## 2. Experimental Procedure

The Ti-15Mo-2.6Nb-3Al-0.2Si-0.12B alloy (in wt.%) was cast via induction skull melting furnace into a 70 mm diameter and 500 mm long ingot at Flowserve Corporation, Dayton, OH. The cast ingots were subjected to hot isostatic pressing (HIP) at 100 MPa at 900 °C for 2 hr. Samples in the form of 10 mm cubes were cut from the ingot and aged at 540 °C / 8 hr and 660 °C / 8 hr.

The microstructure characterization was performed using a 30 keV field emission JEOL JSM-7000F scanning electron microscope (SEM), a 200 keV field emission FEI F20 $G^2$ F20 Supertwin (scanning) transmission electron microscope ((S)TEM) and an Imago Scientific Instruments Local Electrode Atom Probe (LEAP®) 3000XSi in a laser pulsing mode. The SEM specimens were metallographically polished to a mirror finish. The TEM foils were prepared by site-specific specimen extraction of the α-Ti region on the TiB precipitate and subsequently thinned using a FEI Quanta 3D dual electron-focus ion beam (FIB) microscope which was equipped with an Omniprobe micromanipulation lift-out system. The details of FIB-based TEM foil preparation can be found elsewhere **[16]**. The atom probe specimens were prepared in a similar manner to the TEM foils via site specific extraction

using the FIB and placing the specimens onto pre-fabricated Si mounting posts. Rather than thinning a rectangular foil cross-section, the atom probe tips were annular ion milled into the appropriate geometric needle shape required for field evaporation. The details of FIB-based atom probe preparation can be found elsewhere **[17]**. In both the TEM and atom probe specimen preparation, the initial cutting was performed at 30 keV with the final milling at 5 keV, which dramatically reduces the Ga ion implantation and surface damage to the specimen **[18]**. The atom probe specimens in the LEAP® were held at a base temperature of 40K and thermal assisted evaporated using a fs laser pulse operated at 0.3 nJ at a pulse rate of 250 kHz. The LEAP analysis chamber was $< 10^{-10}$ Torr. The atom probe data was analyzed using the IVAS$^{TM}$ 3.4 software developed by Imago scientific Instruments. The compositional profiles are represented as proximity historgrams (proxigrams) with a step size of 0.1 nm **[19]**.

## 3. Results

**Figure 1 (a)** shows a low magnification backscattered electron SEM image of the sample heat treated at 660 ºC / 8 hr. **Figure 1 (b)** is the magnified image of the region indicated by the box in **Figure 1 (a)**. In this image, the boride precipitate is clearly visible in the grain boundary with the α-Ti precipitate forming a globular morphology around the boride phase. Note that in the magnified image, the boride is viewed in a cross-section, *i.e*. the boride phases are acicular in structure **[5-8, 12-15, 20, 21]**. **Figures 1 (c), (d) and (e)** are the energy dispersive spectroscopy (EDS) maps of boron, molybdenum, and aluminum, respectively, obtained from the region corresponding to **Figure 1 (b)**. The boron map clearly shows the enrichment of boron in the precipitate and a depletion of boron in the grain boundaries. The lath-like depletions of the molybdenum signal, **Figure 1(d)**, can be seen in the matrix which shows the regions of α-Ti precipitation since molybdenum is a beta-stabilizing alloy **[3]**.

Similar to boron, molybdenum is depleted in the grain boundaries. Interestingly, the aluminum map does not show significant depletion in the grain boundaries. Similar to molybdenum, the aluminum signal is depleted in the boride particle as compared to the matrix. Qualitatively, there is an enrichment of aluminum signal around the boride particle, *i.e.* the location of the α-Ti precipitate morphology, which is consistent that aluminum is an alpha stabilizing addition **[3]**.

Unlike the 660 $^{o}$C heat treatment, the 540 $^{o}$C specimen showed a strikingly different α-Ti morphology. **Figures 2 (a) and (b)** are the low magnified and high magnified images of the precipitation of α-Ti off of the TiB precipitate. In this image the acicular long-axis structure of the boride around the α-Ti is clearly observable. In addition, the α-Ti has precipitated as long needle-like laths, rather than being globular, from the TiB phase.

**Figure 3 (a)** shows a bright field TEM image of the sample aged at 660 ºC / 8 hr. Within the β-Ti matrix, two different precipitates are visible in **Figure 3 (a)**. **Figure 3 (b)** shows a selected area electron diffraction (SAED) pattern obtained from precipitate 1, and it can be consistently indexed as the titanium monoboride (TiB) (B27 orthorohmbic structure, a=6.12 Å, b=3.06 Å, and c=4.55 Å structure **[22]**) from the zone axis of $[010]_{TiB}$. In **Figure 3 (b)**, streaks can be observed along the $[200]_{TiB}$. These streaks are attributed to the stacking faults formed on the $(001)_{TiB}$ plane of the TiB phase in **Figure 3(a)** as reported previously **[6, 12, 14, 15, 20]**. Precipitates off of the TiB phase consist of a few grains. The precipitates 2, 3 and 4 formed directly off of the TiB phase, and are in direct contact with the $(100)_{TiB}$, $(101)_{TiB}$ or $(10\bar{1})_{TiB}$ trace, as seen in **Figure 3(a)**. **Figure 3 (c)** shows the selected area diffraction patterns obtained from a region including the β-Ti matrix and precipitates 2, which is off of the TiB phase. Note that the SAED pattern was taken from the zone axis of $[111]_{\beta\text{-}Ti}$. As shown in **Figure 3 (c)**, the precipitate 2 off of the TiB phase is characterized as α-Ti phase

(hexagonal closed packed structure, a= 2.95 Å and c= 4.55 Å **[22]**). Although the α-Ti within the grain have an orientation relationship with the β-Ti matrix as described as $(0001)_{\alpha-Ti}//(1\bar{1}0)_{\beta-Ti}, [11\bar{2}0]_{\alpha-Ti}//[111]_{\beta-Ti}$, **[23]**, such an orientation relationship could not be observed between the α-Ti precipitates off of the TiB phase and the β-Ti matrix.

The SAED pattern in **Figure 4 (a)** was taken from a region including TiB phase and precipitate 4 in direct contact with the $(100)_{TiB}$ trace in **Figure 3(a)**. The corresponding key diagram is shown in **Figure 4 (b)**. From **Figures 4 (a) and (b)**, the α-Ti phase precipitate has an orientation relationship with the TiB particle of $(0001)_{\alpha-Ti}//(001)_{TiB}, [11\bar{2}0]_{\alpha-Ti}//[010]_{TiB}$ (OR I) as reported in references **[14, 15]**. Examination of a number of precipitates has shown that there is the same orientation relationship between the TiB phase and the α-Ti phase in direct contact with the $(100)_{TiB}$ trace. **Figures 4 (c) and (d)** shows the SAED pattern obtained from a region including the TiB phase and a precipitate in direct contact with the $(101)_{TiB}$ or $(10\bar{1})_{TiB}$ trace (precipitate 3 in **Figure 3(a)**), and the corresponding key diagram. The precipitate in direct contact with the $(101)_{TiB}$ or $(10\bar{1})_{TiB}$ trace is also characterized as the α-Ti phase and has a different orientation relationship from the one between the TiB and the α-Ti phase in direct contact with the $(100)_{TiB}$ trace. The OR can be described as $(01\bar{1}0)_{\alpha-Ti}//(101)_{TiB}, [11\bar{2}0]_{\alpha-Ti}//[010]_{TiB}$ (OR II). The α-Ti phase in direct contact with the $(10\bar{1})_{TiB}$ trace has various orientation relationships with the TiB phase. **Figure 4 (e) and (f)** shows the SAED pattern obtained from another region including the TiB phase and α-Ti phase (whose micrograph is not shown) in direct contact with the $(101)_{TiB}$ or $(10\bar{1})_{TiB}$ trace. The OR can be described as $(01\bar{1}1)_{\alpha-Ti}//(001)_{TiB}, [11\bar{2}0]_{\alpha-Ti}//[010]_{TiB}$ (OR III).

**Figure 5 (a)** shows a mass spectrum obtained from the 660 $^{o}$C heat treated sample

acquired from the LEAP®. There were some potential peak overlaps between $Si^{2+}$ and $N^{1+}$ and $Fe^{2+}$ and with $Si^{1+}$ and $Al^{1+}$. However, since the alloy is intentionally added with silicon, the possible small trace amounts of iron and nitrogen impurity peaks were neglected; hence, the silicon concentrations reported could be slightly larger than the true composition. In addition, hydrogen, which can be seen in the spectrum, has not been included in the compositional profile analysis. Hydrogen is a known vacuum contaminate and is difficult, if not impossible, to determine if it is intrinsic to the processed material or resulted from either specimen preparation or during the LEAP® field evaporation analysis.

**Figure 5 (b)** is the 3D atom map reconstruction of the TiB/α-Ti interface obtained. The top side is the TiB phase while the bottom is α-Ti. Between these two phases, there is an isoconcentration interface of 14.5 at. % boron. **Figures 5 (c) and (d)** are the normal projected proxigrams through the TiB/α-Ti interface. As shown in **Figure 5 (c)**, the aluminum and oxygen are enriched in α-Ti phase and depleted in the boride. In contrast, the molybdenum and niobium are enriched in the boride phase. This is consistent with literature that aluminum and oxygen are α-Ti stabilizers where as molydiumn and niobium are β-Ti stabilizers **[3]**. Interestingly, carbon, an α-Ti stabilizer, is at a higher concentration in the TiB phase as compared to α-Ti. It is also shown in this figure that silicon is enriched at the TiB/α-Ti interface with a Gibbsian interfacial excess, Γ, of 0.487 atoms/$nm^2$ **[24]**. There is negligible silicon content in the TiB phase.

**Figure 6 (a)** shows a bright field TEM image of the specimen aged at 540 ºC / 8 hr. The precipitate 1 is in direct contact with the needle like precipitate 2. **Figure 6 (b)** shows the SAED pattern obtained from precipitate 1. The SAED pattern is consistent with that of the TiB phase from the $[111]_{TiB}$ zone axis. **Figure 6 (c)** shows the micro-beam diffraction pattern obtained from a needle-like phase off of the TiB phase (precipitate 2). From the micro-beam

diffraction pattern, the precipitate 2 can be identified as the α-Ti phase from the zone axis of $\left[\bar{2}113\right]_{\alpha-Ti}$. In the $[111]_{TiB}//\left[\bar{2}113\right]_{\alpha-Ti}$ TEM viewing direction, **Figure 6 (b) and (c)**, no clear orientation relationship was observed. Upon stereographically rotating this viewing projection to the two parallel viewing directions of $\left[11\bar{2}0\right]_{\alpha-Ti}//[010]_{TiB}$, the orientation relationship of $\left(01\bar{1}1\right)_{\alpha-Ti}//(200)_{TiB}$ and $\left[11\bar{2}0\right]_{\alpha-Ti}//[010]_{TiB}$ (OR IV) was found. A coarse secondary phase indicated by arrow 3 in **Figure 6 (a)** and has also been identified as the α-Ti phase and is nucleating along the grain boundary. This coarse α-Ti did not have clear orientation relationship with the TiB phase.

**Figure 7** is an atom map that captures the TiB/α-Ti and α-Ti/β-Ti interfaces for the 540 $^{o}$C / 8 hr. specimen. The concentration proxigrams in **Figures 7 (b) and (c)** are through the TiB/α-Ti interface. Similar to the previous TiB/α-Ti profile in **Figure 5** for the 660 $^{o}$C / 8 hr specimen, the minor elements' distribution in the two phases are similar except there does not appear to be any appreciable Si concentration nor enrichment in the phases or interfaces. In contrast, the α-Ti/β-Ti interface, **Figure 7 (d)**, shows an appreciable higher level of silicon than the former interface, with an enrichment of silicon at its interface. The silicon concentration is higher in the β-Ti phase than that of the α-Ti phase, which is consistent with the literature that silicon is a β-Ti stabilizer and tends to segregate to the grain boundaries **[3]**. In addition, silicon was found to be enriched at the α-Ti/β-Ti interface with a Gibbsian interfacial excess was 1.3 atoms/nm$^2$. Another data set from the 540 $^{o}$C / 8hr. specimen is shown in **Figure 8**. The atom map clearly shows the triple junction between the TiB/α-Ti/β-Ti phases. The corresponding proxigrams are shown in **Figures 8 (b) through (e)**. The profiles are similar to those observed in **Figure 7**, in that the silicon appears to be preferentially located between the TiB/β-Ti phases. The molybdenum and niobium segregate to the β-Ti

phase while carbon is preferentially found in the TiB phase, **Figure 8 (c)**. The counting statistics of these profiles are not as high as the previous profiles analysis in **Figure 7** explaining the fluctuations observed. The atom map data set of **Figure 8** is included to assist in the description of the silicon migration during α-Ti coarsening described below.

## 4. Discussion

In the present work, we have investigated the α-Ti phase precipitation off of TiB particles in the Ti-15Mo-2.6Nb-3Al-0.2Si-0.12B (wt.%) alloy aged at 660 / 8 hr and 540 ºC / 8 hr. The morphology of the α-Ti is strongly dependent upon the heat treatment temperature, *i.e.* needle-like at 540 $^{o}$C verses globular at 660 $^{o}$C. In each case, a unique orientation relationship between the α-Ti and TiB phase, which have not been reported in the previous works, were observed. The TiB phase can provide a low energy heterogeneous nucleation site for the α-Ti phase. The needle-like α-Ti precipitates on the TiB phase has an orientation relationship that is different than that of the grain boundary nucleated α-Ti (precipitate 3 in **Figure 6**). From these results, we can understand that the TiB phase provides for unique heterogeneous nucleation sites for the precipitation of the α-Ti phase. With respect to the growth of the precipitated α-Ti phase that nucleated at the TiB particle, the differences in morphologies (needle-like verses globular) is likely because of kinetics. As the temperature is increased from 540 $^{o}$C to 660 $^{o}$C, the needles will coarsen. The globular structure of α-Ti is the coarsening of those needles into the observed globular structure. Thus, the 660 $^{o}$C heat treatment is an over-aged micrograph of the 540 $^{o}$C microstructure.

As shown in **Figure 3**, the α-Ti precipitate at 660 °C / 8 hr is in direct contact with the $(100)_{TiB}$ and $(101)_{TiB}$ trace whereas the α-Ti precipitate at 540 °C/8 hr in **Figure 6** is in contact with the $(101)_{TiB}$ trace. The acicular shaped TiB phase with the B27 orthorhombic structure is

reported to grow along its $[010]_{TiB}$ direction because of the high packing density and strong bonds within the $(010)_{TiB}$ plane **[20]**. From the SEM and TEM micrographs and previous literature reports **[20]**, the morphology of the TiB phase is a hexagonal shaped needle with its prismatic planes being $(100)_{TiB}$, $(101)_{TiB}$ and $(10\bar{1})_{TiB}$ **[20]**. Considering these morphology characteristics of the TiB phase, we can conclude that the α-Ti phases, seen in **Figures 3 and 6,** precipitates on the $(100)_{TiB}$, $(101)_{TiB}$ and $(10\bar{1})_{TiB}$ plane of the TiB phase, respectively.

In a previous report for a Ti-6Al-4V alloy, only one TiB/α-Ti orientation relationship of $(001)_{TiB}//(0001)_{\alpha-Ti}$, and $[010]_{TiB}//[11\bar{2}0]_{\alpha-Ti}$ (OR I) has been reported **[14, 15]**. In the present study, we have revealed that this orientation relationship could be observed between the TiB phase and the α-Ti phase precipitating on the $(100)_{TiB}$ plane of the TiB. **Figure 9** shows the schematic illustration of this orientation relationship viewed from the $[100]_{TiB}$ zone axis. Since this orientation relationship gives good lattice matching between the α-Ti phase and the TiB phase on the $(100)_{TiB}$ plane, the α-Ti phase precipitating on the $(100)_{TiB}$ plane can nucleate and grow maintaining this orientation relationship.

On the other hand, the α-Ti phase precipitating on $(101)_{TiB}$ and $(10\bar{1})_{TiB}$ plane of TiB phase has various orientation relationships with the TiB phase such as $(01\bar{1}0)_{\alpha-Ti}//(101)_{TiB}$ and $[11\bar{2}0]_{\alpha-Ti}//[010]_{TiB}$ (OR II), and $(01\bar{1}1)_{\alpha-Ti}//(001)_{TiB}$ and $[11\bar{2}0]_{\alpha-Ti}//[010]_{TiB}$ (OR III) as observed in **Figure 4**. In addition, for the needle like α-Ti phase seen in the sample at 540 °C / 8 hr in **Figure 6**, the orientation relationship, OR IV, can be described as $(01\bar{1}1)_{\alpha-Ti}//(200)_{TiB}$ and $[11\bar{2}0]_{\alpha-Ti}//[010]_{TiB}$ when it is viewed from $[010]_{TiB}$ zone axis. These three orientation relationships yield that $(11\bar{2}0)_{\alpha-Ti}$ and the $(010)_{TiB}$ planes are always parallel to each other. This can be understood because the plane spacing of $(11\bar{2}0)_{\alpha-Ti}$ and

$(010)_{TiB}$ plane are 1.475 and 1.517 Å with only 2% difference. However, the good lattice matching cannot be obtained between the TiB and α-Ti phase on the $(101)_{TiB}$ and $(10\bar{1})_{TiB}$ plane if the OR I, which is observed in the α-Ti phase forming on the $(100)_{TiB}$, is maintained. Therefore, the orientation relationship between TiB and α-Ti are not limited to only one if the α-Ti precipitates on $(101)_{TiB}$ and $(10\bar{1})_{TiB}$ plane of TiB.

In the present study, we have addressed how the α-Ti phase grows at the TiB precipitate. **Figure 10** shows the schematic illustration of the growth process of the α-Ti phase nucleating at the TiB particle. When α-Ti precipitates off of the TiB, it does not form a clear orientation relationship, like the Burgers orientation relationship **[23]**, with the surrounding β-Ti matrix, as seen in **Figure 3 (c)**. The orientation relationship for these α-Ti precipitates is with the TiB particles. Consequently, as the α-Ti coarsens in the β-Ti matrix around the TiB particle, an incoherent interface is formed between the α-Ti/β-Ti. In this case, the α-Ti needles that grow on the same TiB plane can easily coarsen to reduce the interfacial energy as shown in **Figure 10**. Eventually, these coarsening needles, on separate planes with distinctly different orientation relationships that depend on the TiB growth plane as seen in **Figure 4**, impinge into each other forming a polycrystalline globular α-Ti phase forms around the TiB particles as shown in **Figure 3 (a)** and illustrated in **Figure 10**.

With respect to the chemistry, the atom probe analysis of the micro-alloying elements was consistent with the literature, *i.e.* alpha stabilizing elements such as aluminum where segregated to the α-Ti phase and beta stabilizing elements like molybdenum and niobium were segregated to the β-Ti phase. Interestingly, the carbon, an alpha stabilizer, was found to be at a slightly higher concentration in the TiB phase than in α-Ti. The most interesting observation was the migration of silicon between the two heat treatments. At 540 $^{o}$C / 8 hr, a

condition where both α-Ti and β-Ti are in contact with the TiB phase, the silicon content enriches the interface between α-Ti/β-Ti but not the α-Ti/TiB. Clearly, the precipitation of α-Ti in β-Ti rejects a portion of silicon and enriches the α-Ti/β-Ti interface. Surprisingly, this silicon interfacial enrichment is not observed for the precipitation of α-Ti at the TiB phase. In contrast, the 660 $^{o}$C / 8 hr specimen does exhibit an enrichment of silicon at the α-Ti/TiB interface. This change is a consequence of α-Ti's coarsening around the TiB phase. As β-Ti is converted into α-Ti, **Figure 10**, the previous retained silicon in β-Ti, which cannot be fully accommodated by the newly formed α-Ti or TiB, migrates to the α-Ti-/TiB interface. Thus, the coarsening behavior of α-Ti into a globular morphology around TiB does affect the microsegrgation of the constituent alloying elements.

**5. Summary**

We have investigated the microstructure of Ti-15Mo-2.6Nb-3Al-0.2Si-0.12B at two different aging temperatures. It was found that at 540 $^{o}$C / 8 hr, α-Ti precipitates as a needle-like structure from the TiB phase. Upon aging at 660 $^{o}$C / 8 hr, the α-Ti coarsens around the TiB phase and forms a globular morphology. SAED patterns revealed two orientations relationships of α-Ti/TiB: $(10\bar{1}1)_{\alpha-Ti}//(011)_{TiB}$ and $[11\bar{2}0]_{\alpha-Ti}//[4\bar{1}1]_{TiB}$ for the one aged at 660°C and $(\bar{2}113)_{\alpha-Ti}//(111)_{TiB}$, and $[01\bar{1}1]_{\alpha-Ti}//[3\bar{4}1]_{TiB}$ for 540 $^{o}$C. By plotting these two orientation relationships onto a $[010]_{TiB}$ sterographic projection, it was concluded that these orientation relationship differences are likely a result of α-Ti precipitating on two different growth planes of TiB. As observed in the micrographs of this paper and reported by others **[5-8, 12-15, 20, 21]**, TiB forms hexagonal shaped fibers with prismatic planes consisting of $(100)_{TiB}$, $(101)_{TiB}$ and $(10\bar{1})_{TiB}$ possible growth surfaces. These planes provide the nucleation

surfaces for α-Ti. Atom probe tomography revealed the expected segregation of alpha and beta stabilizing elements to their respected phases. Interestingly, carbon, an alpha stabilizer, was enriched in the TiB phase as compared to the α-Ti phase when in contact. The coarsening of α-Ti around the TiB phase also resulted in the migration of silicon from the α-Ti/β-Ti interfaces to the α-Ti/TiB interfaces.

**Acknowledgements:**

This research was performed under AFRL contract FA8650-04-D-5235. The Tecnai $G^2$ F20 Super-twin TEM and laser upgrade to the LEAP 3000XSi was acquired through the National Science Foundation Major Instrumentation Program, NSF-DMR-0421376 and NSF-DMR-0722631, respectively.

**References**

[1] Brewer WD, Keith Bird R, Wallace TA, Mater. Sci. and Eng. A 1998; 243; 299

[2] Ivasishin OM, Markovsky PE, Matviychuk YV, Semiatin SL, Ward CH, Fox S, J. Alloys Comp. 2008: 457; 296

[3] Polmear IJ, Light Alloys, fourth ed., Butterworth-Heinemann, Oxford, 2006, pp. 97-204

[4] Nayeb-Hashemi AA and Clark JB. Phase Diagrams of Binary Magnesium Alloys. Materials Park, OH: ASM international; 198

[5] Cherukuri B, Srinivasan R, Tamirisakandala S, Miracle DB. Scripta Mater. 2009: 60; 496

[6] Fan Z, Miodownik A, Acta Mater. 1996: 44;93

[7] Yamamoto T, Otsuki A, Ishihara K, Shingu PH. Mater. Sci. and Eng. A, 1997: 239-240; 647

[8] Zhang X, Lü W, Zhang Z, Wu R. Scripta Mater. 1999: 41; 39

[9] Ma ZY, Tjong SC, Gen L. Scripta Mater. 2000: 42; 367

[10] Tanya M, Godfrey T, Goodwin PS, Malcolm Ward-Close. Adv. Eng. Mater. 2: 2000; 85

[11] Banerjee R, Collins PC, Fraser HL. Adv. Eng. Mater. 4: 2002; 847

[12] Feng H, Zhou Y, Jia D, Meng Q, Comp. Sci. and Tech. 2004: 64; 2495

[13] Tamiriskandala S, Bhat RB, Tiley JS, Miracle DB. 2005: 53; 1421

[14] Hill D, Banerjee R, Huber D, Tiley J, Fraser HL. Scripta Mater. 2005: 52; 387

[15] Li DX, Ping DH, Lu YX, Ye HQ. Mat. Letter 1993: 16; 322

[16] Giannuzzi LA and Stevie FA, Micron 1999: 30(3); 197

[17] Thompson K, Lawrence D, Larson DJ, Olson JD, Kelly TF, Gorman B, Ultramicroscopy 2007: 107; 131.

[18] Giannuzzi LA, Microscopy and Microanalysis Proceedings 2006: 12; 1260 (CD)

[19] Hellman OC, Vandenbroucke JA, Rusing J, Isheim D, Seidman DN, Microscopy and

Microanalysis 2000: 6(5); 437

[20] Lu W, Zhang L, Zhang X, Wu R, Sakata T, Mori H, J. Alloys. Comp. 2001: 327; 240

[21] Lieberman SI, Gokhale AM, Tamirisakandala S, Mater. Characterization 2007:58; 527

[22] Villars P and Calvert LD, Pearson's Handbook of Crystallographic Data for Intermetallic Phases (second ed.), ASM International, Materials Park, OH, 1991

[23] Burgers WG, Physica 1934: 1; 561

[24] Phys. Rev. B 1993: 48; 6724

**Figure 1**

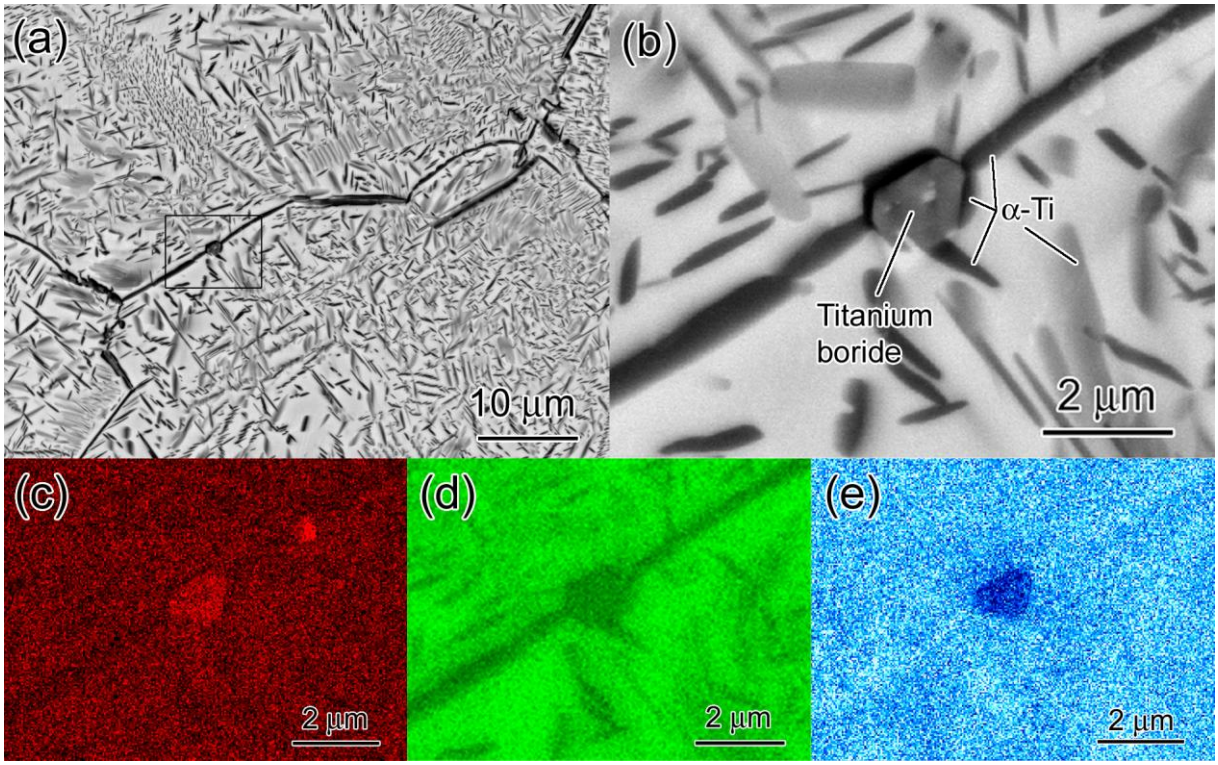


Figure 1: (a) Backscattered electron SEM image after aging at 660 ºC / 8 hr. (b) Magnified image obtained from a region surrounded by solid line in (a). (c), (d) and (e) are EDS mapping image of boron, molybdenum and aluminum, respectively, obtained from a region corresponding to (b).

**Figure 2**

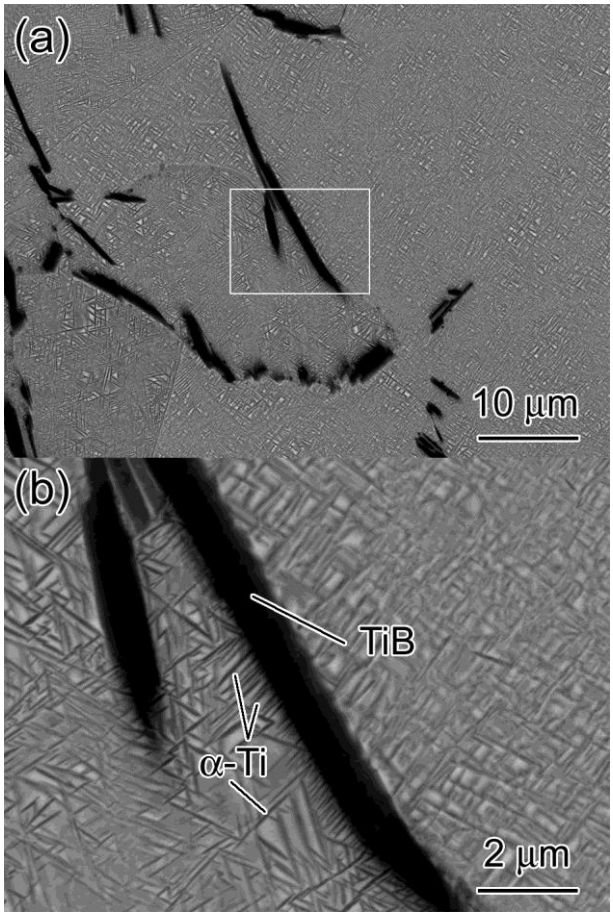


Figure 2: (a) Backscattered electron SEM after aging at 540 ºC / 8 hr. (b) is the magnified image obtained from a region surrounded by solid line in (a). Note the needle-like α-Ti precipitates on the TiB phase.

**Figure 3**

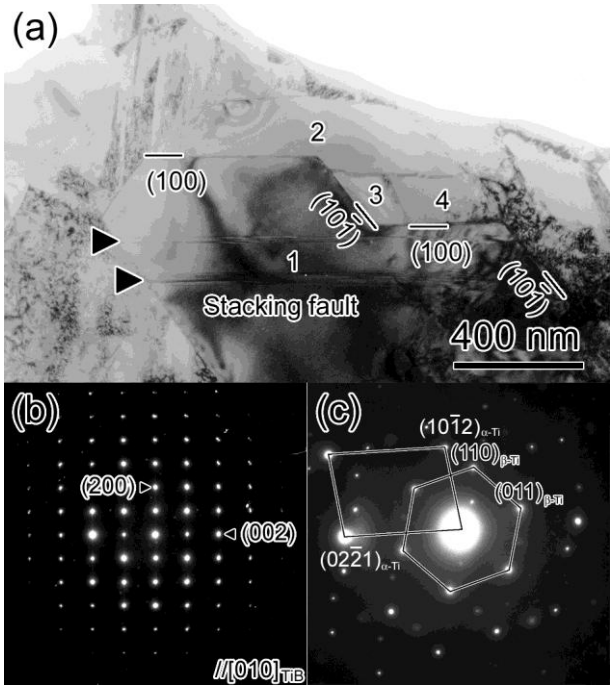


Figure 3: (a) Bright field TEM image showing α-Ti precipitates nucleating at TiB particles obtained from a sample aged at 660ºC for 8 hr. (b) and (c) are selected area electron diffraction (SAED) patterns obtained from precipitate 1, a region including precipitate 2 and β-Ti matrix. Note that (a) was taken from the zone axis of $[010]_{\beta\text{-}Ti}$. This image indicates the impingement of a-Ti precipitates 2, 3, and 4 into the globular polycrystalline α-Ti morphology around TiB.

**Figure 4**

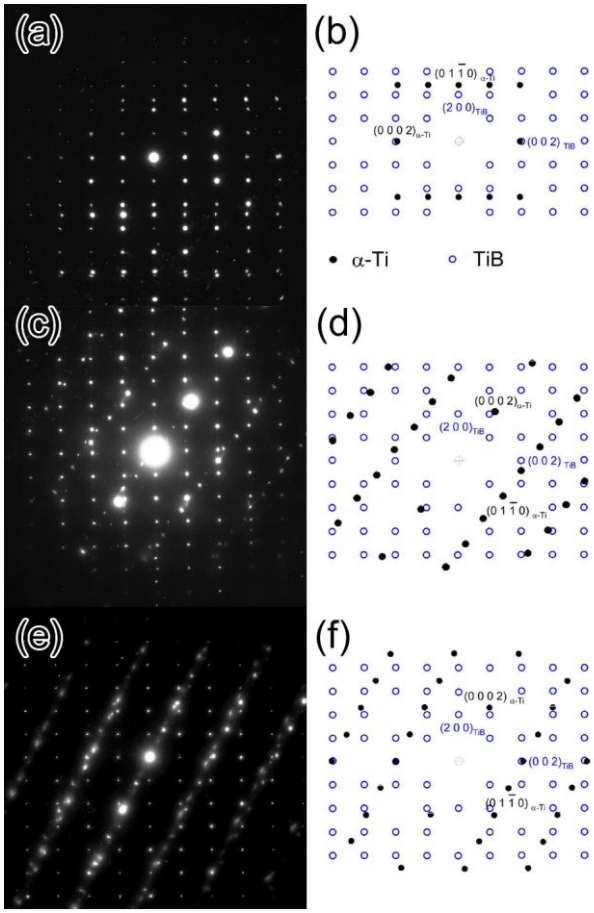


**Figure 4**: (a) and (b) are selected area electron diffraction (SAED) pattern and corresponding key diagram obtained from a region including precipitate 1 and 2 in Figure 3. (c) and (d) are selected area diffraction (SAD) pattern and corresponding key diagram obtained from a region including precipitate 1 and 3 in Figure 3. (c) and (d) are SAED pattern and corresponding key diagram obtained from a region including another TiB phase and α-Ti phase in direct contact with the $(10\bar{1})_{TiB}$ trace of the TiB phase.

**Figure 5**

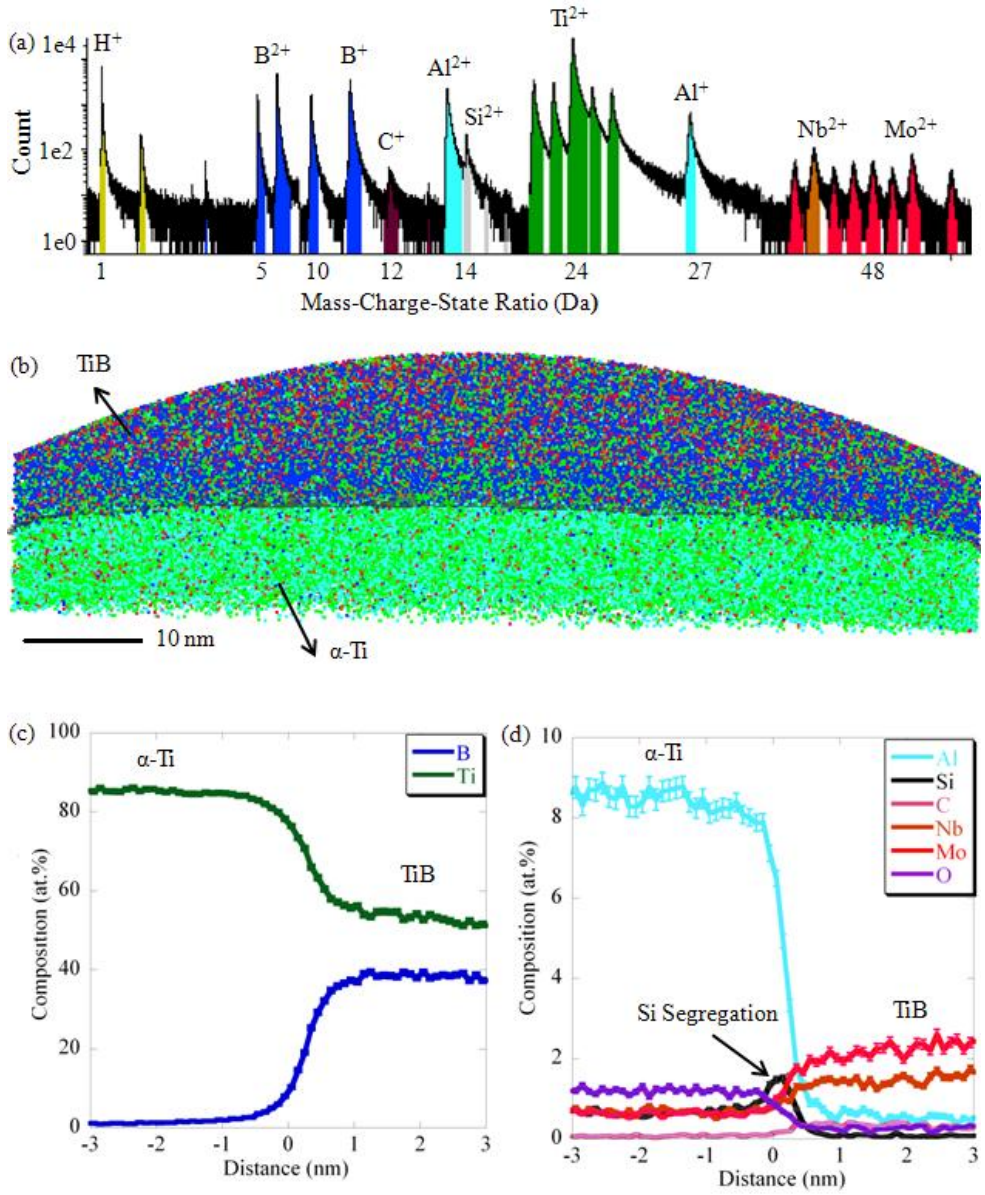


Figure 5: (a) Mass spectrum obtained from the sample aged at 660 $^{o}$C / 8hr, (b) 3D atom map obtained from TiB / α-Ti interface analyzed from the sample aged at 660 °C, (c) and (d) are concentration profiles of B and Ti, and Al, H, Si, C, Nb and Mo analyzed from (b).

**Figure 6**

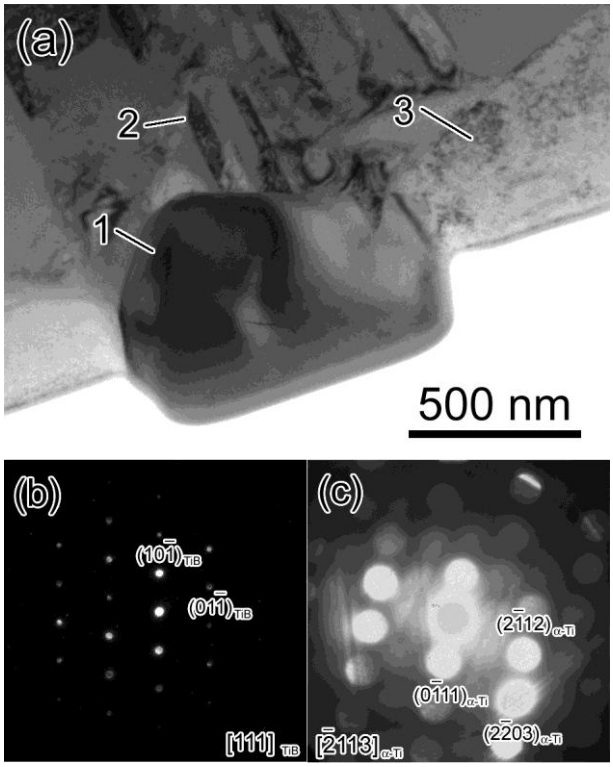


Figure 6: (a) Bright field TEM image showing α-Ti precipitate (precipitate 2) off of TiB phase (precipitate 1) obtained from a sample aged at 540ºC / 8h. (b) and (c) are selected area diffraction (SAD) patterns obtained from the precipitates 1 and micro-beam diffraction pattern obtained from precipitate 2.

**Figure 7:**

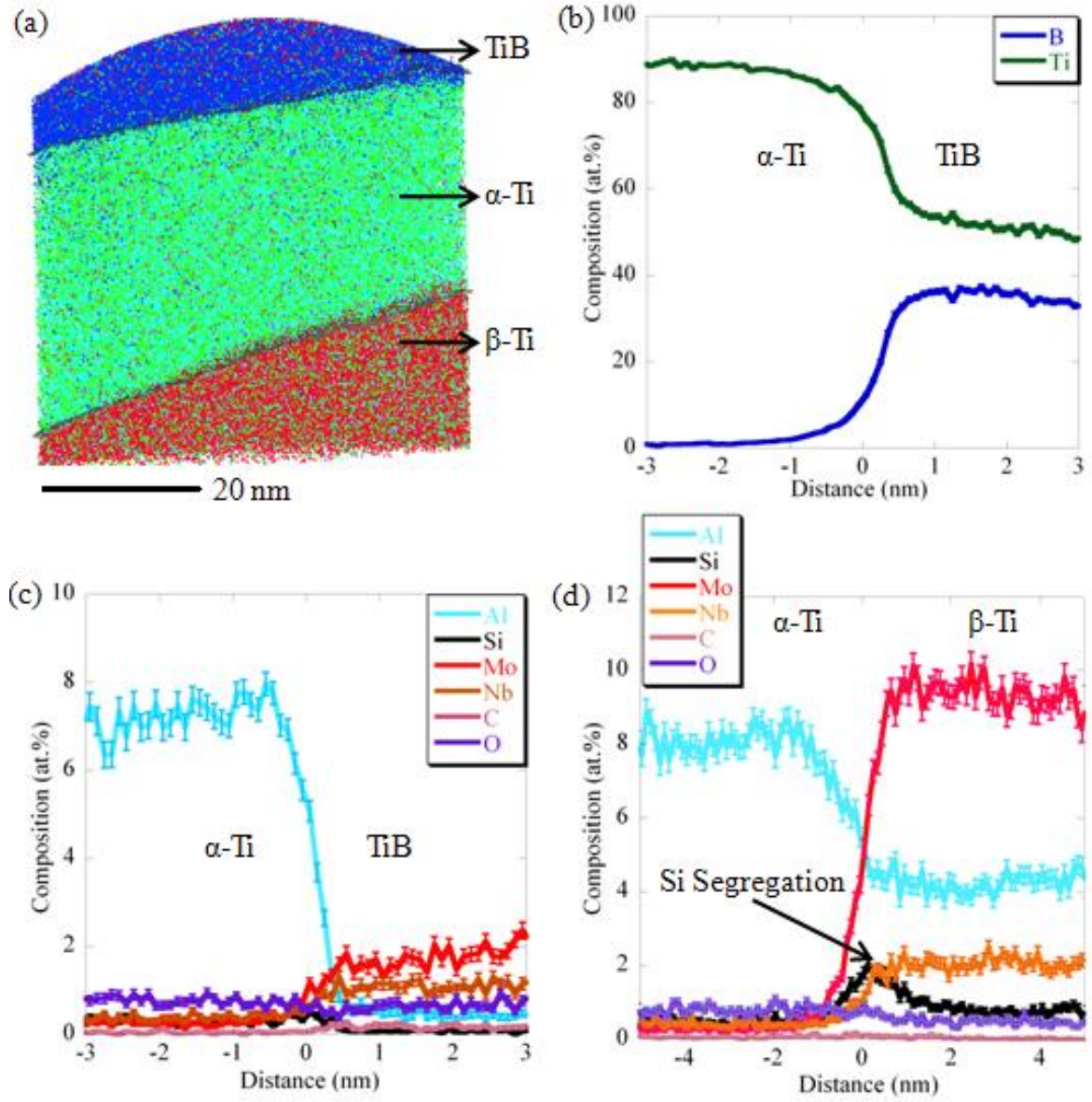


Figure 7; (a) 3D atom map obtained from TiB / α-Ti interface analyzed from the sample aged at 540 °C / 8 hr, (b) and (c) are concentration profiles of B and Ti, and Al, H, Si, C, Nb and Mo analyzed in (a).

**Figure 8**

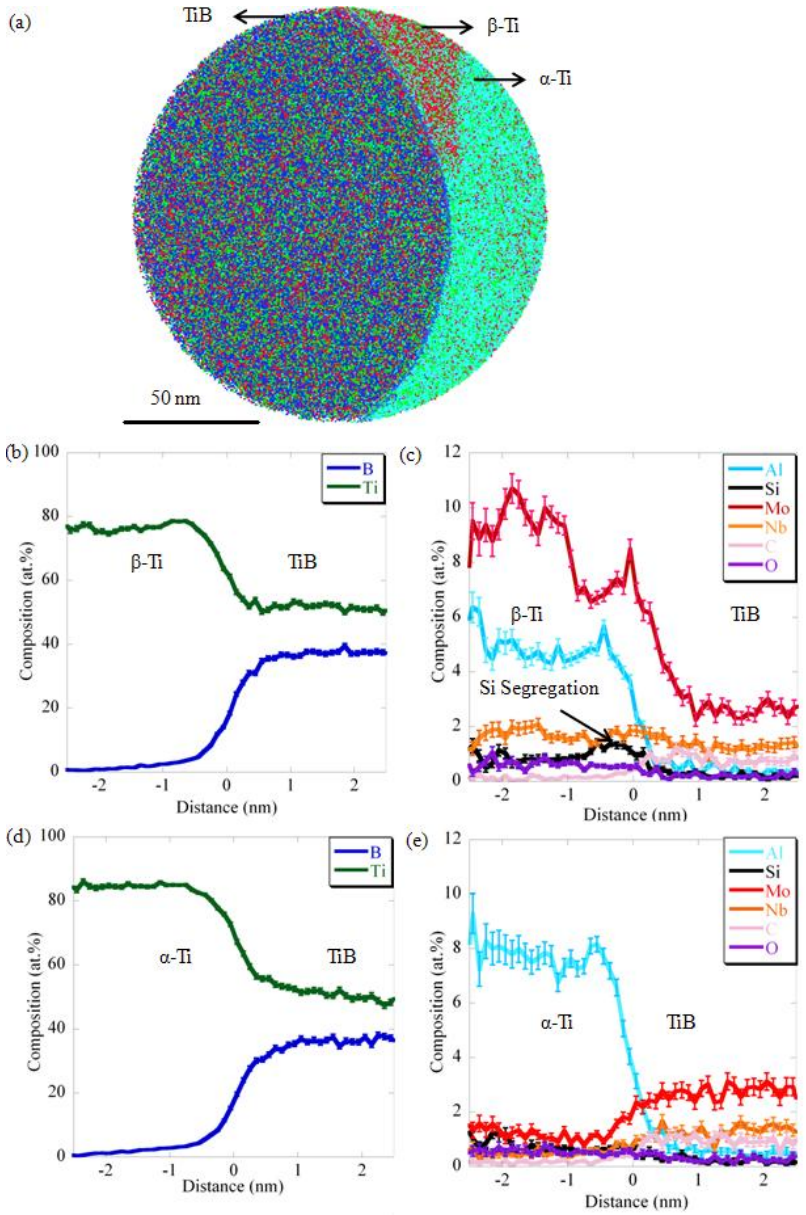


Figure 8: (a) 3D atom map obtained from TiB / α-Ti interface analyzed from the sample aged at 540 °C, (b) and (c) are concentration profiles of B and Ti, and Al, H, Si, C, Nb and Mo analyzed from TiB/α-Ti interface and (d) is the one of of B and Ti, and Al, H, Si, C, Nb and Mo analyzed from TiB/β-Ti interface.

**Figure 9**

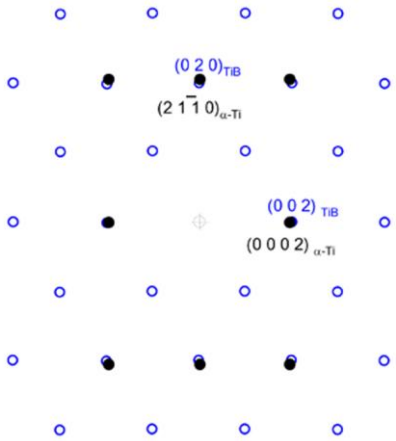


Figure 9: Orientation relationship of $(001)_{TiB}$ //$(0001)_{\alpha-Ti}$, and $[010]_{TiB}$ //$[11\bar{2}0]_{\alpha-Ti}$ (OR I) viewed from $(100)_{TiB}$ zone axis

**Figure 10**

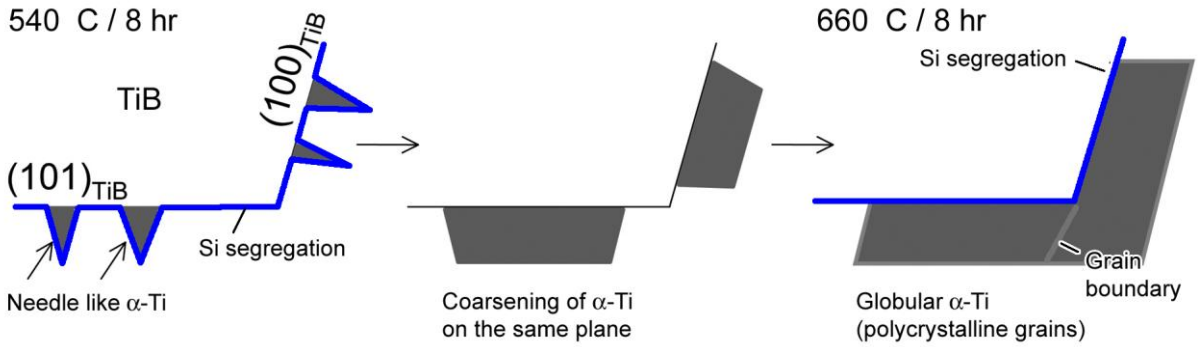


Figure 10: Schematic illustration of the growth process of α-Ti phase nucleating at TiB phase viewed from $[010]_{TiB}$ zone axis. Note that the blue line shows the segregation of silicon around the TiB particle and α-Ti precipitates off of the TiB phase.